Compact, Wideband, Planar Filtenna with Reconfigurable Tri-Polarization Diversity

Ming-Chun Tang, *Senior Member, IEEE*, Dajiang Li, Xiaoming Chen, *Student Member, IEEE*, Yang Wang, Kunzhi Hu, and Richard W. Ziolkowski, *Fellow*, *IEEE*

***Abstract*—A compact, wideband, planar filtenna with reconfigurable tri-polarization diversity is presented. The operating mechanisms of its band-pass filter and its bandwidth enhancement are explained through a step-by-step design evolution. Its feed network consists of three J-shaped probes, a Wilkinson power divider, and phase-shifters. Reconfigurability is achieved by integrating four pairs of p-i-n (PIN) diodes into it. Three polarization-reconfigurable states: linear polarization (LP) and left-hand (LHCP) and right-hand (RHCP) circular polarization, are dynamically controlled by those PIN diode switches. A prototype was fabricated, assembled, and tested. It has a compact size: 0.48 $\lambda_0 \times 0.45\ \lambda_0$, and is low profile: 0.096 λ_0. The measured results, in good agreement with their simulated values, demonstrate that the filtenna has a wide -10-dB impedance bandwidth ($|S_{11}| \leq -10$ dB): 15.6%, that completely encompasses the axial ratio bandwidths (AR ≤ 3 dB) of the two CP states. The realized gain values over this bandwidth: 7.7 ± 0.5 dBi, are very stable for all three dynamical states. Furthermore, the filtenna exhibits good out-of-band rejection performance characteristics.**

***Index Terms*—Compact, filtennas, planar antennas, polarization diversity, reconfigurable antennas, wideband**

I. Introduction

Filtennas combine filters and antennas into a single module [1-4]. With proper co-design one can reduce the interconnection lengths and losses between the filter and radiating elements to attain a more compact, efficient, and lower cost RF front-ends. Moreover, filtennas with their inviting features of frequency selectivity and out-of-band rejection to effectively improve the signal-to-noise ratio. They are quite suitable for complex electromagnetic environments.

Spectrum resources have been growing increasingly scarce with the rapid development of wireless communication technologies. Moreover, as the number of wireless devices within a space-limited front-end platform increases, and the electromagnetic environments in which they operate are becoming increasingly more complicated. To address these issues, advanced types of reconfigurable antennas have been developed with innovative techniques [5]. Polarization- reconfigurable antennas have proved to be an appropriate choice. They increase the system capacity, reduce multi-path fading, and enhance anti-interference [6]. Generally, the methods that achieve polarization-reconfigurable antennas can be divided into the following three categories. The first is to reconfigure their radiating elements, e.g., insert p-i-n (PIN) diodes into slots [7]-[9] or add perturbing stubs in them [10]. The second is to reconfigure their parasitic, periodic structures, e.g., mechanically adjust a metasurface [11] or insert varactor diodes into an electromagnetic band gap (EBG) structure [12]. The third is to employ reconfigurable feed networks, e.g., insert PIN diodes into their feed networks [13]-[15] or introduce adjustable self-phase-shifter structures to alter the signal pathways [16].

It is highly desirable to empower filtennas with polarization reconfigurability for practical applications. A polarization reconfigurable filtenna has many advantages, e.g., it would have a more compact size, an enhanced system capacity, and an improved anti-interference capability. However, there have been only a few of them reported to date, i.e., [17]-[19]. The waveguide filtenna in [17] achieved reconfigurable linear (LP) and left-hand (LHCP) and right-hand (RHCP) polarization states. Different from this three-dimensional (3-D) waveguide configuration, two-dimensional (2-D) polarization reconfigurable microstrip patch filtennas were presented in [18] and [19]. In [18], a planar reconfigurable patch filtering antenna achieved similar tri-polarization diversity using a proximity-coupled feed that yielded band-pass performance characteristics. In [19], a microstrip filtering antenna with dual-polarization diversity was realized by placing a reconfigurable band-pass coupled-resonator filter structure below the radiating patch. However, these reported planar filtennas have an inherent drawback, i.e., their designs require a separate, rather integrated band-pass filter. This approach makes their operational bandwidth: 0.8 % in [18] and 4.5 % in [19], much narrower than a standard patch antenna with the same volume.

In this Communication, a compact, wideband, planar filtenna with reconfigurable tri-polarization diversity is developed. The operating mechanisms that produce its band-pass filter properties and its bandwidth enhancement are explained using an evolutionary series of passive planar patch antenna designs with different feed technologies and different numbers of patch layers. In contrast to the reconfigurable two CP-state systems reported in [19], the optimized polarization reconfigurable filtenna possesses three switchable polarization states, i.e., LP, LHCP, and RHCP states. Moreover, its size, $0.48\ \lambda_0 \times 0.45\ \lambda_0$, is more compact and it has a much wider operational bandwidth, 15.6%, than the related systems disclosed in [18] and [19]. Furthermore, the filtenna exhibits good out-of-band rejection performance characteristics. A prototype was fabricated, assembled, and tested. The measured results are in good agreement with their simulated values.

Manuscript received on May 09, 2018; revised on Jul. 13, 2018, on Sep. 24, 2018, on Dec. 25, 2018, on Mar. 02, 2019, and on Apr. 22, 2019; and accepted on Apr. 29, 2019.

This work was supported in part by the National Natural Science Foundation of China contract number 61471072, in part by the Funding of the Innovative Leading Talents in Science and Technology of Chongqing contract number CSTCCXLJRC201705, in part by Funding of the Young Backbone Teachers in Colleges and Universities of Chongqing contract number 0307001104102,in part by the Opening Subject of State Key Laboratory of Millimeter Waves under Contract K201732, and in part by the Australian Research Council grant number DP160102219.

M. -C. Tang, D. Li, X. Chen, Y. Wang, and K. Hu are with the Key Laboratory of Dependable Service Computing in Cyber Physical Society Ministry of Education, College of Communication Engineering, Chongqing University, Chongqing 400044, China, and also with the State Key Laboratory of Millimeter Waves, Nanjing 210096, China (e-mail: tangmingchun@cqu.edu.cn);

R. W. Ziolkowski is with the University of Technology Sydney, Global Big Data Technologies Centre, Ultimo NSW 2007, Australia (e-mail: richard.ziolkowski@uts.edu.au).

II. Evolution of the Passive Filtenna

Four initial planar antenna designs led to the final compact wideband filtenna. They were: (I) direct-probe-fed antenna with a single-layer patch; (II) L-shaped-probe-fed antenna with a single-layer patch; (III) J-shaped-probe-fed antenna with a single-layer patch; and (IV) J-shaped-probe-fed antenna with dual-layer patches. The top row of subplots in Fig. 1 illustrates the configurations of the five antennas in sequence for ease of comparison. The bottom subplot gives the realized gain values as functions of the source frequency for all five antennas.

First, there is no filtering response in Antenna I as was anticipated from [20] and [21]. It only has one resonant mode in its passband, which is produced by the radiating patch. Second, when the L-shaped-probe is introduced in Antenna II, a weak radiation null in the lower stopband is generated. As a result, the out-of-band suppression level is improved to a certain extent. One finds that the capacitive coupling of the L-shaped-probe to the patch is responsible for this one radiation null. Third, the L-shaped feed probe is evolved into a J-shaped one in Antenna III. It consists of the original lower stub and an additional connected upper stub. As indicated by the green dot-line curve, a new radiation null is observed. This additional null is produced by the capacitive coupling between the upper stub and the patch. It is very useful since it provides the sharp skirt selectivity found at the upper band edge. One might argue that a good band-pass filter performance characteristic has already been achieved. However, the observed band-pass bandwidth is actually seriously limited because there is only one resonant mode in the passband.

Fourth, a parasitic patch is added right above the radiating patch in Antenna IV in order to attain a wider passband while maintaining the good band-pass filter performance. As shown by the red dash-dot-line curve, the presence of a second resonant mode is produced by the parasitic patch being adjacent to the radiating one, i.e., it expands the operational bandwidth. Finally, Antenna V includes a pair of U-slots etched symmetrically on the lower patch to obtain yet another radiation null as shown in the black solid-line response. This radiation null further improves the skirt selectivity at the upper band-edge [22], [23]. Furthermore, it is clear that Antenna V produces the sharpest out-of-band suppression at that upper stop-band. Therefore, it possesses the best band-pass filtering performance characteristics when compared to the previous designs in this evolutionary sequence.

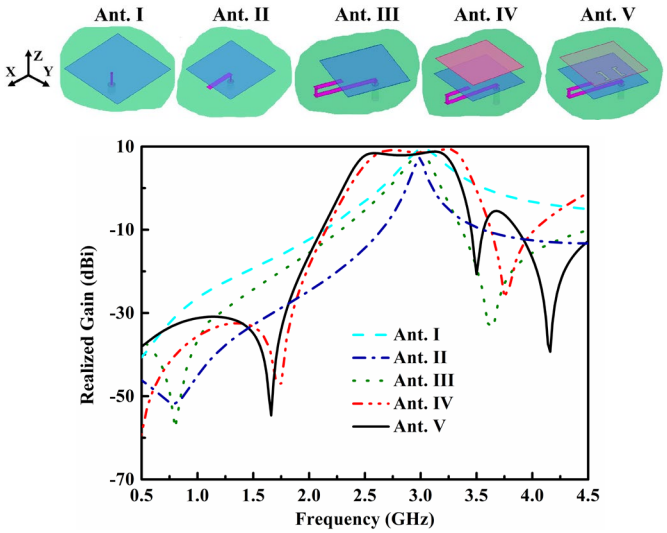

Fig. 1. The passive filtenna evolution. The configuration of all five antennas are indicated in the top row of subplots. The corresponding simulated realized gain values versus the excitation frequency are indicated in the bottom subplot.

III. The Filtenna Configuration and Operation

The elaborated J-shaped probe feed structure of the passive filtenna design illustrated in Antenna V of Fig. 1 can be transformed into a reconfigurable version with three dynamic current pathways equivalent to the J-shaped feed that will realize the desired LP, LHCP, and RHCP states. The filtenna and its switchable feed structure are described below; its reconfiguration operating mechanisms are discussed in Section V. All substrates in the design are Rogers RT/Duroid 5880 with a relative dielectric constant ε_r = 2.2, loss tangent tan δ =0.0009, a 0.017 mm copper cladding thickness, and 0.787 mm dielectric thickness. All layers are square and the same size: $L_1 \times W_1 = 120 \times 120$ mm^2.

A. The Filtenna Configuration

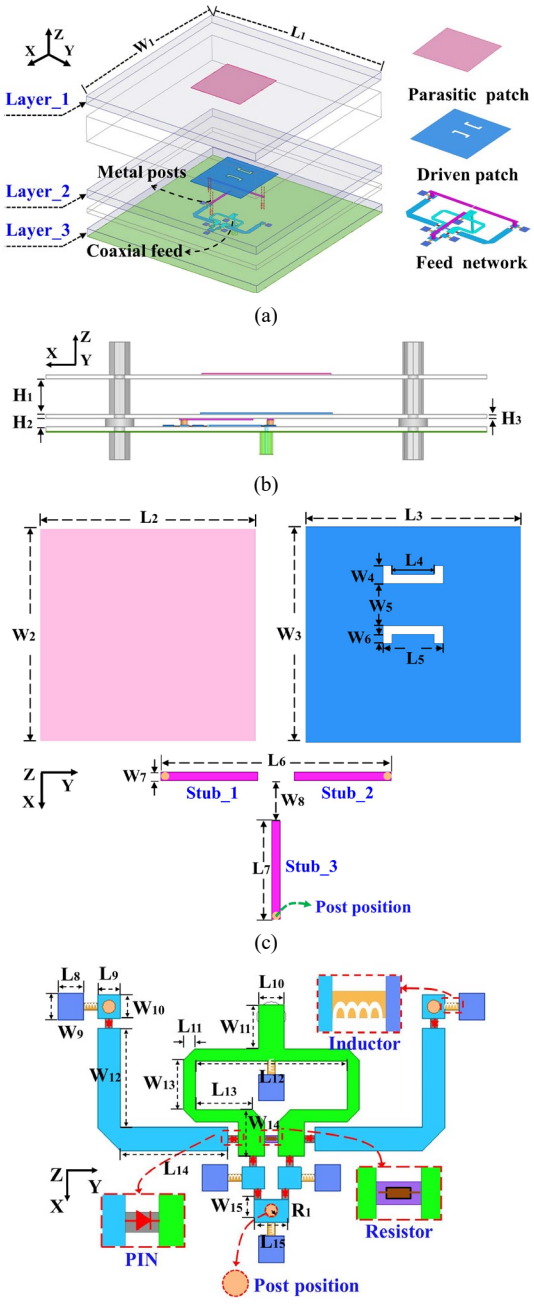

Fig. 2 Filtenna configuration and its design parameters. (a) 3-D isometric view. (b) Side view. (c) Upper surface of Layer_1 and Layer_2 and the lower surface of Layer_2. (d) Upper surface of Layer_3.

Fig. 2 shows the filtenna configuration. As illustrated in Figs. 2(a) and (b), it consists of three square substrate layers which are labeled from the top to the bottom: Layer_1, Layer_2 and Layer_3. The air gap between Layer_1 and Layer_2 has the height H_1; it is optimized to attain a good impedance match. As shown in Fig. 2(c), a square parasitic patch and a driven patch are printed on Layer_1 and Layer_2, respectively. They are both centered on those layers and have the sizes: $L_2 \times W_2$ and $L_3 \times W_3$, respectively. As depicted in Figs. 2(c) and (d), the reconfigurable feed network has three parts: a Wilkinson power divider, a set of phase-shift strips, and three coupling stubs. The Wilkinson power divider (green) and the phase-shift strips (blue) are all located on the upper surface of Layer_3. The three coupling stubs (magenta), labeled Stub_1, Stub_2 and Stub_3, have the same size: $L_7 \times W_7$ and are mounted on the lower surface of Layer_2. They capacitively couple energy to the driven patch. The coupling stubs and the phase-shift strips are connected by three metal posts (yellow) with height H_2 = 1.0 mm and radius R_1 = 0.75 mm. Moreover, the connection points in the feedline and stubs are indicated in Figs. 2(c) and (d).The square ground is located on the lower surface of Layer_3. The optimized design parameters are detailed in Table I.

The signal input to the Wilkinson power divider is split into two equal-amplitude output signals. The output ends of the power divider are connected by a resistor (purple) that is 100 ohm in a 0603 package. It provides the requisite isolation between the two output signals. A 50 Ω coaxial cable with an inner conductor radius R_2 = 0.65 mm was selected to feed the filtenna. Four polyamide pillars, as shown in Fig. 2(b), were used to maintain the relative vertical distances between the three layers and to ensure the mechanical stability of the filtenna during the measurement process.

TABLE I OPTIMIZED DESIGN PARAMETERS OF THE POLARIZATION-RECONFIGURABLE FILTENNA (DIMENSIONS IN MILLIMETERS)

L1 =120	*L2 = 35*	*L3 = 36*	*L4 = 7.0*
L5 = 10	*L6 = 40.4*	*L7 = 20*	*L8 = 3.0*
L9 = 2.65	*L10 = 3.05*	*L11 = 1.4*	*L12 = 17.7*
L13 = 6.65	*L14 = 12.5*	*L15 = 4.0*	*W1 =120*
W2 = 35	*W3 = 36*	*W4 = 3.0*	*W5 = 10*
W6 = 1.5	*W7 = 1.5*	*W8 = 4.0*	*W9 = 3.0*
W10 = 2.65	*W11 = 5.0*	*W12 = 11.35*	*W13 = 5.6*
W14 = 5.4	*W15=2.65*	*H1 = 6.5*	*H2 = 1*
R1 = 0.75	*R2=0.65*	*H3=0.787*	*NULL*

B. DC Biasing of the PIN Diodes

There are four pairs of PIN diodes employed in the feed network to reconfigure the polarization. For an easier description, we have numbered these diodes as D1&D1′, D2&D2′, D3&D3′, and D4&D4′ in Fig. 3. Each diode can be forward biased to its ON state with a DC voltage of 0.95 V. It is in its OFF state if left unbiased. To feed the DC biasing voltage (P1-P6) into the diodes, six square DC pads are etched close to the feedline. They are connected to it via six RF-blocking inductors, which prevent any RF signal from entering the DC bias network. Because of the inherent low-frequency filtering performance of the proposed filtenna, DC blocking capacitors were omitted. Infineon PIN diodes (BAR64–02V) in a SC79 package and 95 nH inductors in a 0603 package were employed. According its datasheet, each PIN diode acts as a 2.1 resistor in its ON state and as a 0.17 pF capacitor in its OFF state [24].

The LP state of the filtenna is produced by supplying the DC biasing voltages: P3 = P4 = 1.0 V are supplied by the "+" pole of DC source, and P5 & P6 = 0 V are supplied by the "-" pole of DC source. Consequently, the diodes D3 & D3′ and D4 & D4′ are in their ON states and the remaining diodes are in their OFF states. The corresponding path that an input signal travels through the feedline is indicated by the red arrows in Fig. 3(a). Since only coupling stub_3 is excited along the -*x*-axis, the LP state is generated along the *x*-axis.

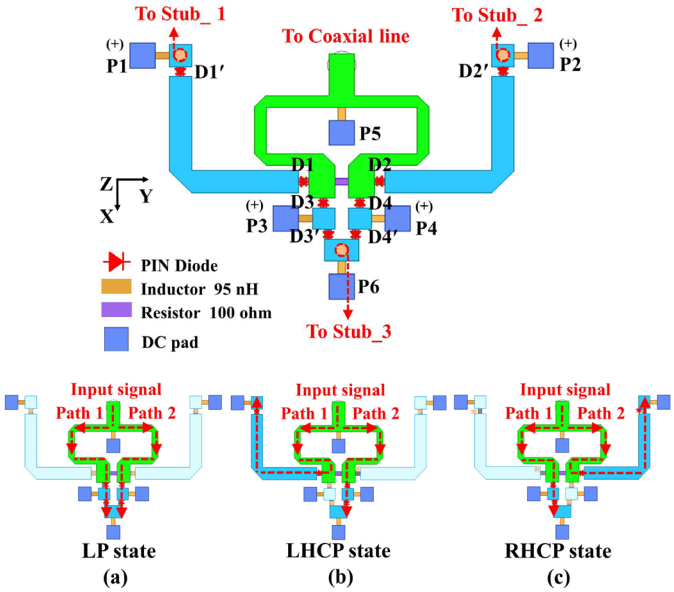

Fig. 3 The operational mechanisms of the reconfigurable feeding network in all three states. (a) LP state. (b) LHCP state. (c) RHCP state. The locations of the PIN diodes on the feed network are indicated in the top subplot. The paths that the input signal travels through the feedline for the three polarization states are indicated by the red arrows in the bottom row of subplots.

TABLE II DC BASING VOLTAGES AND THE DIODE STATES REQUIRED TO ACTIVATE THE DIFFERENT POLARIZATION STATES OF THE FILTENNA

	Diodes states				*DC basing voltage (V)*				
	D1& D1′	*D2& D2′*	*D3& D3′*	*D4& D4′*	*P1*	*P2*	*P3*	*P4*	*P5&P6*
LHCP	ON	OFF	OFF	ON	2	0	0	1	0
RHCP	OFF	ON	ON	OFF	0	2	1	0	0
LP	OFF	OFF	ON	ON	0	0	1	1	0

According to the design principles reported in [25], a CP antenna is achieved by feeding two orthogonal LP radiators with a π/2 phase shift. For the purpose of generating the LHCP state, the voltages: P1 = 2.0 V, P4 = 1.0 V, and P5 & P6 = 0V, turn ON the diodes D1 & D1′, D4 & D4′, while the remaining diodes are OFF. The corresponding path that an input signal travels through the feedline is illustrated in Fig. 3(b). It is easily observed that the length difference of the two paths is approximately one-quarter wavelength, which yields the requisite π/2 phase difference. Moreover, both coupling stub_1 along the +*y*-axis and stub_3 along the -*x*-axis are then excited at the same time. As a consequence, the LHCP state is generated. Similarly, the input signal travels the path through the feedline detailed in Fig. 3(c) when the proper voltages are applied to the corresponding PIN diodes. One observes that coupling stub_2 along the -*y*-axis and stub_3 along the -*x*-axis are excited. Consequently, two orthogonal LP states are excited with equal amplitude and a π/2 phase difference between them, thus generating the RHCP state.

Note that the excited phase-shift strips are indicated in dark blue and the rest are in light blue in all three subplots of Fig. 3 for easy observation. The polarization states of the filtenna, the corresponding diode states, and their DC basing voltages are summarized in Table II.

IV. Simulated and Measured Results

The optimized reconfigurable filtenna shown in Fig. 2 was fabricated, assembled, and measured. This prototype is shown in Fig. 4. The reflection coefficient was measured by an Agilent Technologies E5071C network analyzer, and an ATTEN TPR3003T-3C regulated DC power supply was adopted for the biasing voltage. The far-field characteristics of the prototype, including its realized gain values, radiation patterns, and axial ratios (ARs), were obtained with a multi-probe spherical near field test anechoic chamber.

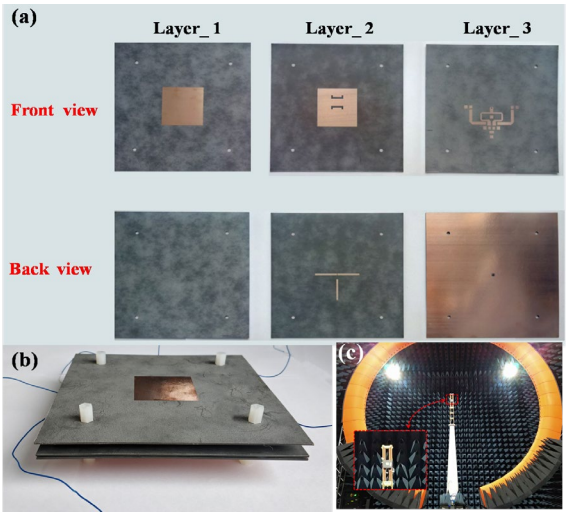

Fig. 4 Fabricated polarization-reconfigurable filtenna. (a) Front and back views of each layer before assembly. (b) 3-D isometric view. (c) Antenna under test (AUT) in the anechoic chamber.

Fig. 5 provides the simulated and measured $|S_{11}|$ and realized gain values of the reconfigurable filtenna for its three polarization states, and the corresponding AR values in its two CP states. Fig. 5(a) demonstrates that the simulated -10-dB fractional impedance bandwidth (FBW) in the LP states is 16.3% (2.65-3.12 GHz) and its measured value is 15.6% (2.71-3.17 GHz). The simulated and measured average realized gain is 8.8 dBi with a ± 0.5 dB fluctuation within the pass-band 2.64-3.17 GHz (18.2%), and 7.7 dBi with a ± 0.5 dB fluctuation within the passband 2.6-3.18 GHz (20.1%).

In Figs. 5(b) and 5(d), the simulated FBW of the LHCP state is 66.4% (1.78-3.55 GHz) and the simulated AR FBW is 34.5% (2.35-3.33 GHz). Thus, the simulated overlapped FBW ($|S_{11}| \leq -10$dB and AR $\leq$ 3dB) is 34.5% (2.35-3.33 GHz). The associated simulated realized gain values are 8.6 dBi with a ±0.5 dB fluctuation within the frequency range 2.65-3.22 GHz (19.4%). This range is completely encompassed within the simulated overlapped bandwidth. Similarly, the measured FBW is 62.6% (1.79-3.42 GHz) and the AR FBW is 27.5% (2.51-3.31 GHz). Thus, the measured overlapped FBW is 27.5% (2.51-3.31 GHz). The measured average realized gain values are 7.7 dBi with a ±0.5 dB fluctuation within the frequency range 2.68-3.24 GHz (19% FBW). Again, this range is completely included in the measured overlapped bandwidth.

In Figs. 5(c) and 5(d), the simulated FBW of the RHCP state is 67% (1.77-3.55 GHz) and the corresponding AR FBW is 38.7% (2.29-3.39 GHz). Thus, the simulated overlapped bandwidth is 2.29-3.39 GHz (38.7%). The associated simulated realized gain is 8.6 dBi with a ±0.5 dB fluctuation within the frequency range 2.65-3.23 GHz (19.7%). This range is also completely encompassed within the simulated overlapped bandwidth. Similarly, the measured FBW is 62.6% (1.79-3.42 GHz) and the AR FBW is 34.9% (2.32-3.3 GHz). Thus, the measured overlapped FBW is 34.9% (2.32-3.3 GHz). The measured average realized gain values are 7.7 dBi with a ±0.5 dB fluctuation within the frequency range 2.71-3.29 GHz (19.3% FBW), which is completely included in the measured overlapped bandwidth.

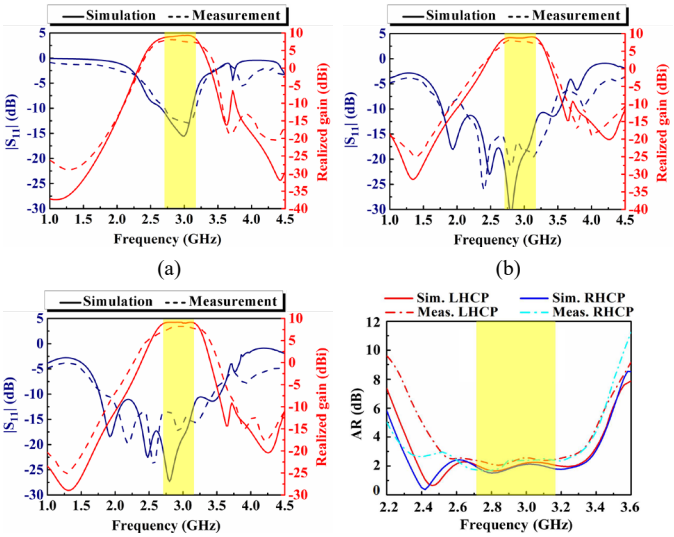

Fig. 5 Simulated and measured $|S_{11}|$, realized gains, and AR values of the reported reconfigurable filtenna. (a) The LP states. (b) The LHCP state. (c) The RHCP state. (d) AR values of the LHCP and RHCP states. The overlapped operational bandwidths of the three states are highlighted in yellow.

Table III Simulated (S) and Measured (M) Results for the Polarization Reconfigurable Filtenna in All Polarization States

Performance \ State		LP	LHCP	RHCP
Impedance FBW (%) ($\|S_{11}\| \leq$ -10dB)	S	16.3	66.4	67
	M	15.6	62.6	62.6
Average realized gain (dBi)	S	8.8	8.6	8.6
	M	7.7	7.7	7.7
AR FBW (%) (AR ≤ 3dB)	S		34.5	38.7
	M		27.5	34.9
1st realized gain null position (GHz) & rejection level (dB)	S	1.14 (37)	1.34 (31)	1.32 (29)
	M	1.28 (29)	1.38 (25)	1.28 (25)
2nd realized gain null position (GHz) & rejection level (dB)	S	3.62 (16)	3.64 (15)	3.64 (14)
	M	3.68 (19)	3.8 (18)	3.92 (15)
3rd realized gain null position (GHz) & rejection level (dB)	S	4.42 (32)	4.26 (20)	4.26 (20)
	M	4.32 (21)	4.02 (19)	4.22 (18)

The reconfigurable filtenna results in all of its three states are summarized in Table III for easy reference. It is noted that the feed network is wideband. When it is operating in the LHCP or RHCP state, the selected two pathways provide a stable phase difference of ~ 90° (70° to 110°) from 2.2 to 3.5GHz. This feature ensures wide impedance and AR bandwidths comparable to those of the LP state. In general, the measured effective FBW (the overlapped operational bandwidth of the three states, highlighted in yellow) of the prototype filtenna is 15.6% (2.71-3.17), which is in good agreement with the simulated value 16.3% (2.65-3.12 GHz). The average realized gain over this effective band is 7.7 dBi with a ±0.5 dB fluctuation for all three polarization states. It is noted that the average measured realized gain values are ~1 dB lower than their simulated ones (8.7 dBi). This

has been confirmed to be largely attributed to the loss of the PIN diodes, as well as to fabrication, assembly, and measurement errors. In each polarization state, three realized gain nulls (one in the lower band and two in the upper band) were present and ensure the measured reasonable out-of-band rejection. In addition, the simulated radiation efficiency (RE) is over 75% across the entire operational band.

The simulated and measured normalized realized gain patterns of the reconfigurable filtenna when it is operating in its LP, LHCP, and RHCP states at 2.9 GHz, which is the center frequency within its effective bandwidth, are shown in Fig. 6. It is clear that its peak gain is in the broadside direction for each polarization and the patterns are symmetrical about this direction. The symmetry follows from the symmetric feedline network and patch structures. The measured co-polarized fields in its LP state are at least 37dB stronger than the cross-polarized counterparts. The measured LHCP (RHCP) fields are at least 17 dB stronger than the opposite RHCP (LHCP) for LHCP (RHCP) states. Furthermore, the measured front-to-back ratio (FTBR) is more than 18 dB for all three polarization states.

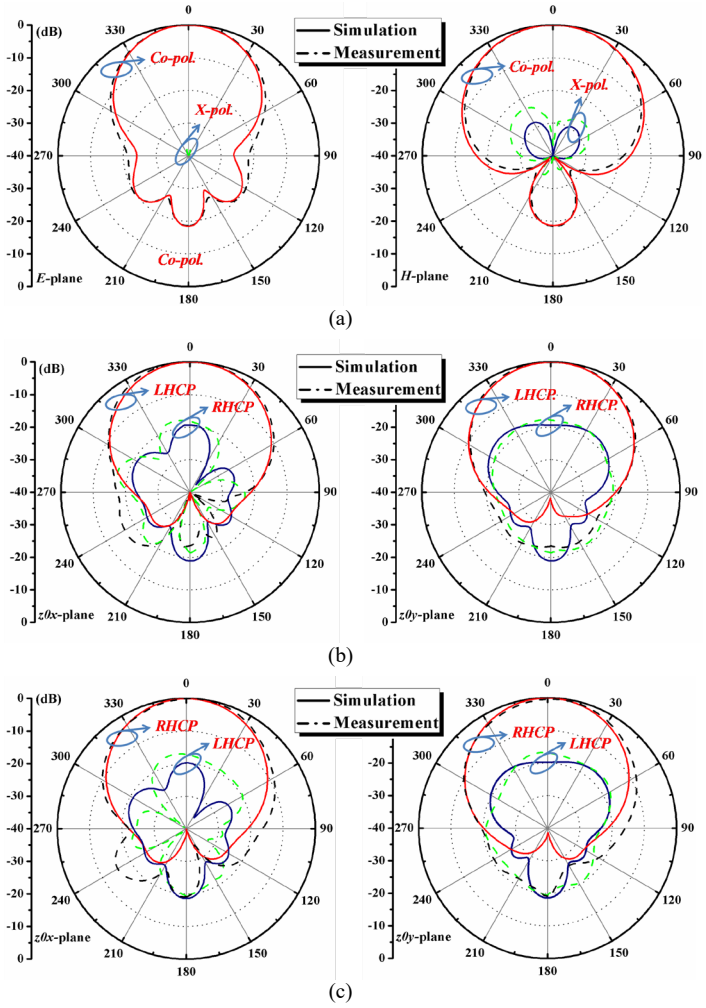

Fig. 6 The simulated and measured normalized realized gain patterns of the prototype filtenna operating at 2.9 GHz for all three of its polarization states. (a) LP state. (b) LHCP state. (c) RHCP state.

As with the filtennas reported in [1-4], our reconfigurable filtenna is an integrated co-design. It is not a simple cascade of multiple devices, i.e., the filter and the antenna. Consequently, it significantly reduces the interconnection losses and costs while taking up much less space. Moreover, the polarization states of our reconfigurable filtenna can be changed quickly, a highly desirable feature shared with those reported in [18] and [19]. Table IV provides a direct comparison with those planar reconfigurable filtennas. Our prototype has not only a more compact transverse size and significantly wider effective bandwidth, but it also possesses flatter realized gain values across its operational band. Moreover, it has significantly higher realized gain values for all three polarization states.

TABLE IV COMPARISONS OF THE PERFORMANCE CHARACTERISTIC OF THE PROTOTYPE POLARIZATION-RECONFIGURABLE FILTENNA WITH RELATED ANTENNAS REPORTED IN THE LITERATURE

Refs.	Transverse size	Height ($*\lambda_0$)	Peak realized gain (dBi)	Effective bandwidth (%)	Polarization states
[18]	$0.69\,\lambda_0 \times 0.59\,\lambda_0 = 0.407\,\lambda_0^2$	0.02	3.01	0.8	LHCP, RHCP, LP
[19]	$0.5\,\lambda_0 \times 0.5\,\lambda_0 = 0.25\,\lambda_0^2$	0.095	6.5	4.5	LHCP, RHCP
Reported Filtenna	$0.48\,\lambda_0 \times 0.45\,\lambda_0 = 0.216\,\lambda_0^2$	0.096	8.2	15.6	LHCP, RHCP, LP

* λ_0 is the free space wavelength corresponding to the center frequency, f_0, of the operational band.

V. RECONFIGURABLE OPERATING MECHANISMS

The reconfiguration operating mechanisms governing the three polarization states of the filtenna were investigated. The current distributions on the upper surface of both the parasitic and driven patches are given in Figs. 7 and 8, respectively, for the filtenna's LP and CP states at the center frequency of its effective bandwidth, 2.9 GHz. For easy interpretation, the directions of the surface currents in each state are highlighted with additional red (referring to the parasitic patch) and blue (referring to the driven patch) arrows. As shown in Fig. 7, the surface currents on these two patches are uniformly oriented along the *x*-axis during the entire period. This behavior confirms that the filtenna radiates a LP field with quite high polarization purity.

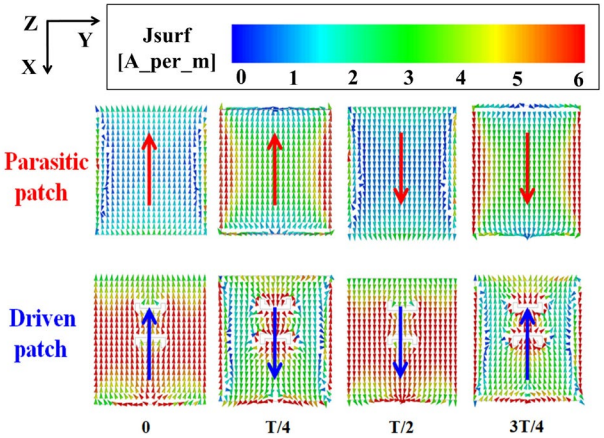

Fig. 7 Surface current distributions on the upper surface of both the parasitic and driven patches of the filtenna over one period T=1/f_0, where f_0 is the center frequency point, 2.9 GHz, of its effective bandwidth when it operates in its LP state.

In a similar manner, the current distributions on the parasitic and driven patches are shown in Fig. 8 for both CP states over one period. The LHCP state is given in Fig. 8(a). The surface currents exhibit a clear clockwise rotation over one period. Similarly, the RHCP state current distributions are shown in Fig. 8(b). They clearly illustrate the expected counter-clockwise behavior.

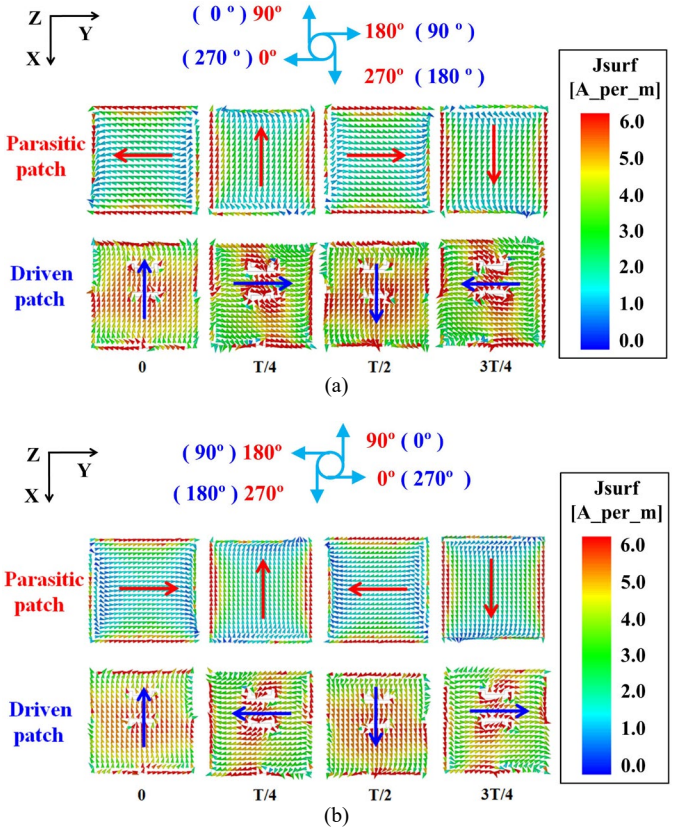

Fig. 8 Surface current distributions on the upper surface of both the parasitic and driven patches of the filtenna over one period T=1/f_0, where f_0 is the center frequency point, 2.9 GHz, of its effective bandwidth when it operates in its CP states. (a) LHCP state. (b) RHCP state.

VI. Conclusion

A compact, wideband, planar, polarization-reconfigurable filtenna with LP, LHCP, and RHCP polarization states was demonstrated. The operating mechanisms attributed to the filtenna design strategy were explained using an evolutionary series of planar patch antenna designs. A set of PIN diodes integrated into the feeding network allows one to dynamically reconfigure its three polarization states. A prototype was fabricated, assembled, and tested. The measured results, in good agreement with their simulated values, demonstrate that the antenna exhibits a wide effective 15.6% FBW centered at 2.9 GHz with a flat broadside average realized gain, 7.7 ± 0.5 dBi, and corresponding simulated RE values over 75% over this operational band. The measured good out-of-band rejection performance characteristics for all three dynamical states were explained. The polarization reconfigurable filtenna design has many potential applications in a variety of wireless communication systems.

References

[1] G. Q. Luo, W. Hong, H. J. Tang; J. X. Chen, X. X. Yin, Z. Q. Kuai, K. Wu, "Filtenna consisting of horn antenna and substrate integrated waveguide cavity FSS," *IEEE Trans. Antennas Propag.*, vol. 55, no. 1, pp. 4933–4939, Jan. 2007.

[2] S. W. Wong, T. G. Huang, C. X. Mao, Z. N. Chen, and Q. X. Chu, "Planar filtering ultra-wideband (UWB) antenna with shorting pins," *IEEE Trans. Antennas Propag.*, vol. 61, no. 2, pp. 948–953, Feb. 2013.

[3] W. Duan, X. Y. Zhang, Y.-M. Pan, J. X. Xu, and Q. Xue, "Dual-Polarized Filtering Antenna With High Selectivity and Low Cross Polarization," *IEEE Trans. Antennas Propag.*, vol. 64, no. 10, pp. 3383–3388, Oct. 2016.

[4] M.-C. Tang, Y. Chen, and R. W. Ziolkowski, "Experimentally validated, planar, wideband, electrically small, monopole filtennas based on capacitively loaded loop resonators," *IEEE Trans. Antennas Propag.*, vol. 64, no. 8, pp. 3353–3360, Aug. 2016.

[5] Y. J. Guo, P. -Y. Qin, S.-L. Chen, W. Lin, and R. W. Ziolkowski, "Advances in reconfigurable antenna systems facilitated by innovative technologies," *IEEE Access*, vol. 6, no. 1, pp. 5780-5794, 2018.

[6] F. Wu and K. M. Luk, "Single-port reconfigurable magneto-electric dipole antenna with quad-polarization diversity," *IEEE Trans. Antennas Propag.*, vol. 65, no. 5, pp. 2289–2296, May 2017.

[7] B. Kim, B. Pan, S. Nikolaou, Y.-S. Kim, J. Papapolymerou, and M. M. Tentzeris, "A novel single-feed circular microstrip antenna with reconfigurable polarization capability," *IEEE Trans. Antennas Propag.*, vol. 56, no. 3, pp. 630–638, Mar. 2008.

[8] Y.-M. Cai, S. Gao, Y. Yin, W. Li, and Q. Luo, "Compact-size low-profile wideband circularly polarized omnidirectional patch antenna with reconfigurable polarizations," *IEEE Trans. Antennas Propag.*, vol. 64, no. 5, pp. 2016–2021, May 2016.

[9] L. Ge, Y. Li, J. Wang, and C.-Y.-D. Sim, "A low-profile reconfigurable cavity-backed slot antenna with frequency, polarization, and radiation pattern agility," *IEEE Trans. Antennas Propag.*, vol. 65, no. 5, pp. 2182–2189, May. 2017.

[10] W. Lin and H. Wong, "Polarization reconfigurable wheel-shaped antenna with conical-beam radiation pattern," *IEEE Trans. Antennas Propag.*, vol. 63, no. 2, pp. 491–499, Feb. 2015.

[11] H. L. Zhu, S. W. Cheung, X. H. Liu, and T. I. Yuk, "Design of polarization reconfigurable antenna using metasurface," *IEEE Trans. Antennas Propag.*, vol. 62, no. 6, pp. 2891–2898, Jun. 2014.

[12] B. Liang, B. Sanz-Izquierdo, E. A. Parker, and J. C. Batchelor, "A frequency and polarization reconfigurable circularly polarized antenna using active EBG structure for satellite navigation," *IEEE Trans. Antennas Propag.*, vol. 63, no. 1, pp. 33–40, Jan. 2015.

[13] Y. Cao, S. W. Cheung, and T. I. Yuk, " A simple planar polarization reconfigurable monopole antenna for GNSS/PCS," *IEEE Trans. Antennas Propag.*, vol. 63, no. 2, pp. 500–507, Feb. 2015.

[14] W. Lin and H. Wong, "Wideband circular-polarization reconfigurable antenna with L-shaped feeding probes," *IEEE Antennas Wireless Propag. Lett.*, vol. 16, pp. 2114–2117, 2017.

[15] Y. Luo, Q.-X. Chu, and L. Zhu, "A low-profile wide-beamwidth circularly-polarized antenna via two pairs of parallel dipoles in a square contour," *IEEE Trans. Antennas Propag.*, vol. 63, no. 3, pp. 931–936, Mar. 2015.

[16] M. Wang, M. R. Khan, M. D. Dickey, and J. J. Adams, "A compound frequency- and polarization reconfigurable crossed dipole using multidirectional spreading of liquid metal," *IEEE Antennas Wireless Propag. Lett.*, vol. 16, pp. 79–82, 2017.

[17] F. Farzami, S. Khaledian, B. Smida, and D. Erricolo, "Reconfigurable linear/circular polarization rectangular waveguide filtenna," *IEEE Trans. Antennas Propag.*, vol. 66, no. 1, pp. 9–15, Jan. 2018.

[18] T. H. Gan, Z. Yang, E. L. Tan, J. X. Lim, M. Q. Huynh, and M. Mayank, "A polarization-reconfigurable filtering antenna system," *IEEE Antennas Propag. Magazine*, vol. 55, no. 6, pp. 198–219, Dec. 2013.

[19] Y. Lu, Y. Wang, S. Gao, C. Hua, and T. Liu, "Circularly polarised integrated filtering antenna with polarisation reconfigurability," *IET Microw. Antennas Propag.*, vol. 11, pp. 2247–2252, Dec. 2017.

[20] I. J. Bhal and P. Bhartia, *Microstrip Antenna*. Dedham, MA: Artech House, 1980.

[21] C. A. Balanis, *Antenna Theory: Analysis and Design*, 3rd edition, New York: Wiley Interscience, 2005.

[22] X. Y. Zhang, W. Duan, and Y.-M. Pan, "High-gain filtering patch antenna without extra circuit," *IEEE Trans. Antennas Propag.,* vol. 63, no. 12, pp. 5883–5888, Dec. 2015.

[23] W.-C. Mok, S.-H. Wong, K.-M. Luk, and K.-F. Lee, "Single-layer single patch dual-band and triple-band patch antennas," *IEEE Trans. Antennas Propag.,* vol. 61, no. 8, pp. 4341–4344, Aug. 2013.

[24] Datasheet for bar64series. Munich, Germany: Infineon Technologies AG81726, 2013.

[25] P. Jin and R. W. Ziolkowski, "Multi-frequency, linear and circular polarized, metamaterial-inspired, near-field resonant parasitic antennas," *IEEE Trans. Antennas Propag.*, vol. 59, no. 5, pp. 1446–1459, May 2011.